Jurnal Teknokes
Homepage: teknokes.org; Vol. 19, No. 2, pp. 061 - 071, June 2026;
e-ISSN: 2407-8964
p-ISSN: 1907-7904

RESEARCH PAPER

OPEN ACCES

Classification of Autism Spectrum Disorder (ASD) in Children Using the VGG19 CNN Model Based on Facial Landmarks of the Eye and Forehead Areas

Arya Suyanda[1], Yunidar Yunidar[1], Melinda Melinda[1], Lailatul Qadri Zakaria[2], Siti Rusdiana[3]

[1] Department of Electrical and Computer Engineering, Universitas Syiah Kuala, Banda Aceh, Indonesia
[2] Faculty of Information Science and Technology, Universiti Kebangsaan Malaysia, Bangi, Selangor, Malaysia
[3] Department of Mathematics, Universitas Syiah Kuala, Banda Aceh, 23111, Indonesia

ABSTRACT

Early detection of Autism Spectrum Disorder (ASD) is a crucial challenge in childhood developmental interventions. Conventional screening methods are often subjective and susceptible to assessor bias. This study proposes an objective solution for automated ASD classification using deep learning. The solution focuses exclusively on the eye and forehead regions. The main contribution of this research is a novel, focused-landmark visualization method that integrates Dlib 68 for adaptive cropping with MediaPipe Face Mesh's high-density topology. It isolates neurobiological biomarkers and eliminates non-contributory facial noise. These specific areas were selected based on the eye avoidance hypothesis, which states that they contain rich diagnostic information and behavioral biomarkers related to the ASD phenotype. In the preprocessing stage, the eye and forehead areas were isolated using Dlib 68 landmark detection. This eliminated background visual noise that could interfere with feature extraction. Next, detailed topological visualization was performed using MediaPipe Face Mesh with 478 landmark points. This served as the model's primary input. The implemented Convolutional Neural Network (CNN) architecture was a VGG19 model trained via transfer learning. Dropout layers were added to improve computational efficiency and prevent overfitting. The model was trained using a primary dataset of 1,238 images from children in Banda Aceh, collected under controlled conditions. The test results showed very promising performance with an overall accuracy of 94.35%. Specifically, the model achieved a recall (sensitivity) of 95.24%, a precision of 93.75%, and an AUC of 0.9831. These findings demonstrate that visualizing reference points in the eye and forehead areas, combined with the VGG19 model, is an effective, accurate, and practical method. This innovation has great potential as an economical and objective early screening tool for people with ASD in the future.

PAPER HISTORY

Received February 18, 2026
Revised March 30, 2026
Accepted April 04, 2026
Published June 13, 2026

KEYWORDS

Autism Spectrum Disorder; Deep Learning; VGG19; Facial Landmarks; Eye-avoidance Hypothesis; MediaPipe Face Mesh; Early Screening

CONTACT:

arya.su@mhs.usk.ac.id
yunidar@usk.ac.id
melinda@usk.ac.id
lailatul.qadri@ukm.edu.my
siti.rusdiana@usk.ac.id

1. INTRODUCTION

Autism Spectrum Disorder (ASD) is a complex neurodevelopmental disorder characterized by persistent deficits in social communication and social interaction, as well as restricted and repetitive patterns of behavior, interests, or activities [2]. These symptoms can manifest as significant challenges in learning, sensory processing, and emotional regulation, ultimately negatively impacting the quality of life of individuals and their families [3] [4] [5]. Given its increasing global prevalence [1] [2], early detection is crucial. Timely intervention has been shown to have a profound positive impact on developmental outcomes, particularly in improving adaptive and communication skills [6] [7]. However, the early diagnosis of ASD faces significant challenges due to the wide heterogeneity of symptoms. Each individual with ASD displays a unique phenotypic profile. For example, while some children exhibit marked verbal delays, others may have proficient speech skills but fail to interpret non-verbal cues such as eye contact [8] [9]. This variability complicates conventional screening methods,which largely rely on clinical observations and questionnaires, which are often subjective, time-consuming, and prone to rater bias [10] [11] [12] [13]. Rapid advances in Artificial Intelligence (AI), particularly Deep Learning (DL), have revolutionized medical data analysis and offer objective solutions to these diagnostic challenges [14] [15] [16] [17] [18]. Transfer Learning techniques, which leverage pre-trained models trained on large datasets, have become a standard approach to addressing the limitations of medical data [19] [20] [21]. In particular, DL-based facial image analysis has emerged as a promising non-invasive method, given that faces contain important biomarker information related to neurodevelopmental disorders [11] [22] [23].

Corresponding author: Yunidar, yunidar@usk.ac.id, Department of Electrical and Computer Engineering,Faculty of Engineering, Universitas Syiah Kuala, Darussalam, Banda Aceh, 23111, Aceh, Indonesia
DOI: https://doi.org/10.35882/jteknokes.v19i2.158

Several recent studies have evaluated the effectiveness of Convolutional Neural Networks (CNNs) in detecting ASD. Previous research has shown that the VGG19 architecture often outperforms other models, including InceptionV3 and DenseNet201 [24]. Specifically, VGG19 achieved 85% accuracy on a child face dataset. Another study by [25] reported that the VGG-19 architecture achieved 96.47% accuracy in classifying facial features in autistic

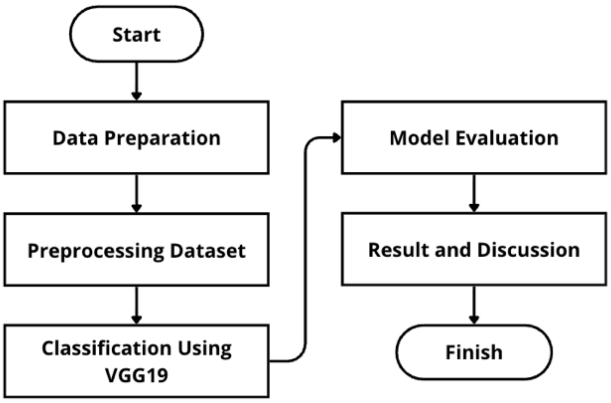

Fig. 1. Workflow of This Study.

children, demonstrating that CNNs are highly effective at recognizing subtle differences that are difficult to distinguish by ordinary visual inspection. To overcome these limitations, geometric feature-based approaches or facial landmarks offer a more targeted analysis. In support of this, previous research has shown that marker feature fusion consistently improves accuracy by combining discriminative geometric information [26]. However, using landmark coordinates alone sometimes fails to capture the richness of visual features compared to image-based methods [27] [28]. To address this gap, a hybrid approach that visualizes landmarks into overlay images of key diagnostic areas is a potential strategy. Biologically, this focus is well-founded because specific craniofacial characteristics in ASD, such a intercanthal distance, have been highlighted in medical research [22] [23]. In addition, the confirmation of the "eye aversion" hypothesis regarding amygdala activity further supports treating the eye area as the most informative Region of Interest (ROI) in the diagnostic process [8].

Based on these research gaps, the main contribution of this study is the application of a modified VGG19 CNN architecture to classify ASD using facial landmark visualizations focused exclusively on the eyes and forehead. The selection of VGG19 was based on its robust architecture, which has been shown to outperform more complex models across various medical and non-medical classification tasks [24] [29] [30]. As illustrated in Fig. 1, raw facial images were processed to isolate the eye and forehead ROIs, then transformed into landmark visual representations using MediaPipe, and finally used as model input. Specifically, this study aims to:

- Design and implement a hybrid method with a modified VGG19 architecture • to address the challenge of detecting ASD using focused landmark visualization data.
- Assess the model's performance using comprehensive metrics such as accuracy, precision, recall, and AUC score, to validate the superiority of this focused approach over conventional full-face methods.

2. MATERIALS AND METHOD

A. Dataset

This study used an independently curated primary dataset consisting of 1,238facial images from 60 child participants (30 with ASD, 30 neurotypical) aged 5–15 years. Subjects were recruited from Special Elementary Schools (SLB) and Public Elementary Schools in Banda Aceh, Indonesia. Each participant contributed approximately 20 images across three expressions (neutral, smiling, sad), yielding a class-balanced dataset

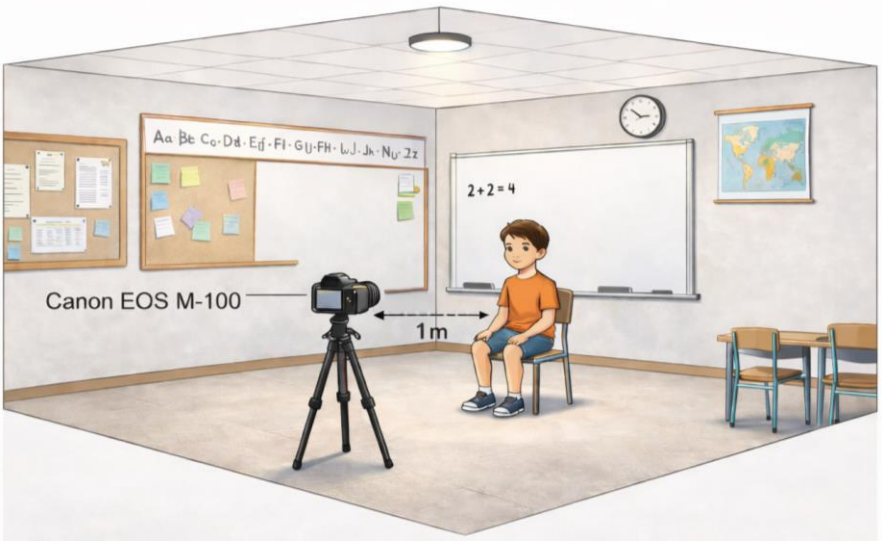

Fig. 2. Controlled environment setup for facial image acquisition.

Corresponding author: Yunidar, yunidar@usk.ac.id, Department of Electrical and Computer Engineering,Faculty of Engineering, Universitas Syiah Kuala, Darussalam, Banda Aceh, 23111, Aceh, Indonesia
DOI: https://doi.org/10.35882/jteknokes.v19i2.158

of 619 ASD and 619 normal images. This balanced distribution is crucial for mitigating prediction bias and ensuring the stability of model evaluation metrics [31] [32]. Data collection was conducted in a controlled environment, with the experimental protocol illustrated in Fig. 2. The acquisition room measured 7m x 7m, with a specific imaging area of 2m x 2m. To ensure consistent image quality, environmental parameters were maintained at 25-27°C and 40–45% humidity, with 30-watt ambient ceiling lighting . Acquisition sessions began at 09:00 and concluded by 12:00, with each participant undergoing a 10–15-minute acclimatization phase to reduce sensory anxiety [6].

The technical setup involved a Canon EOS M-100 camera placed on a tripod at a distance of 1 m from the subject. A 17-inch LCD screen was used to display visual stimuli to elicit the desired facial expressions, while a black curtain was installed to block external light interference. This strict protocol aimed to minimize environmental noise that could distort the feature extraction process [25]. This study has obtained official ethical approval (Ethics Code: 036/EA/FK/2025) and written informed consent from the parents/guardians of the students in accordance with medical data integrity standards [11]. Exclusion criteria were strictly applied to eliminate subjects with acute illnesses or comorbid disorders such as intellectual disability, cerebral palsy, and Down syndrome. For ASD participants, all images were captured immediately before the start of their scheduled therapeutic intervention sessions to ensure an authentic baseline phenotype.

B. Dlib 68 Face Landmark Detection

At the outset of each image processing session, the Dlib library is used to implement anô Ensemble of Regression Trees algorithm. This method was chosen due to its proven ability to perform fast and robust facial pose estimation [33]. In the proposed system architecture, Dlib's landmark detection is applied early in the session as a spatial localization mechanism to precisely determine anatomical Regions of Interest (ROIs), rather than as a direct feature extractor for classification. The algorithm maps 68 fiducial points on the face, with vector coordinates for eyebrow landmarks (points 17–26) extracted as geometric anchors for adaptive cropping. This cropping isolates the eyes and forehead, removing lower-face artifacts and irrelevant background. Such noise elimination reflects a data-centric approach that values clean input data to enhance diagnostic model performance [34]. Restricting the ROI to the upper face has strong neurobiological support. This approach aligns with the “eye avoidance” hypothesis, linked to amygdala responses in individuals with ASD [8]. Additionally, recent morphological studies highlight significant physical biomarkers in the upper ocular and craniofacial areas, such as variations in intercanthal distance [22] and optic nerve morphometric features [35], both of which are strongly correlated with ASD diagnosis.

C. MediaPipe Face Mesh

After the ROI isolation stage, the cropped image is then transformed using the MediaPipe Face Mesh module. Unlike conventional face detection methods that rely on only a few points, MediaPipe offers high topological resolution by detecting 478 3D landmark points. This point density captures important microexpression details and subtle curvatures in the periorbital area, an advantage validated in comparative feature extraction studies [28]. At this stage, the raw photographic image is combined with the original image I. This creates a visual representation of the feature as a geometric map. The process overlays P marker points and their connectivity on the original image. A consistent semantic coloring scheme is used: (1) Green for facial surface tessellation, (2) Blue and Red for eyebrow and eye contours, and (3) Highlighter Green for the iris area. This visualization strategy is based on previous research. Such research

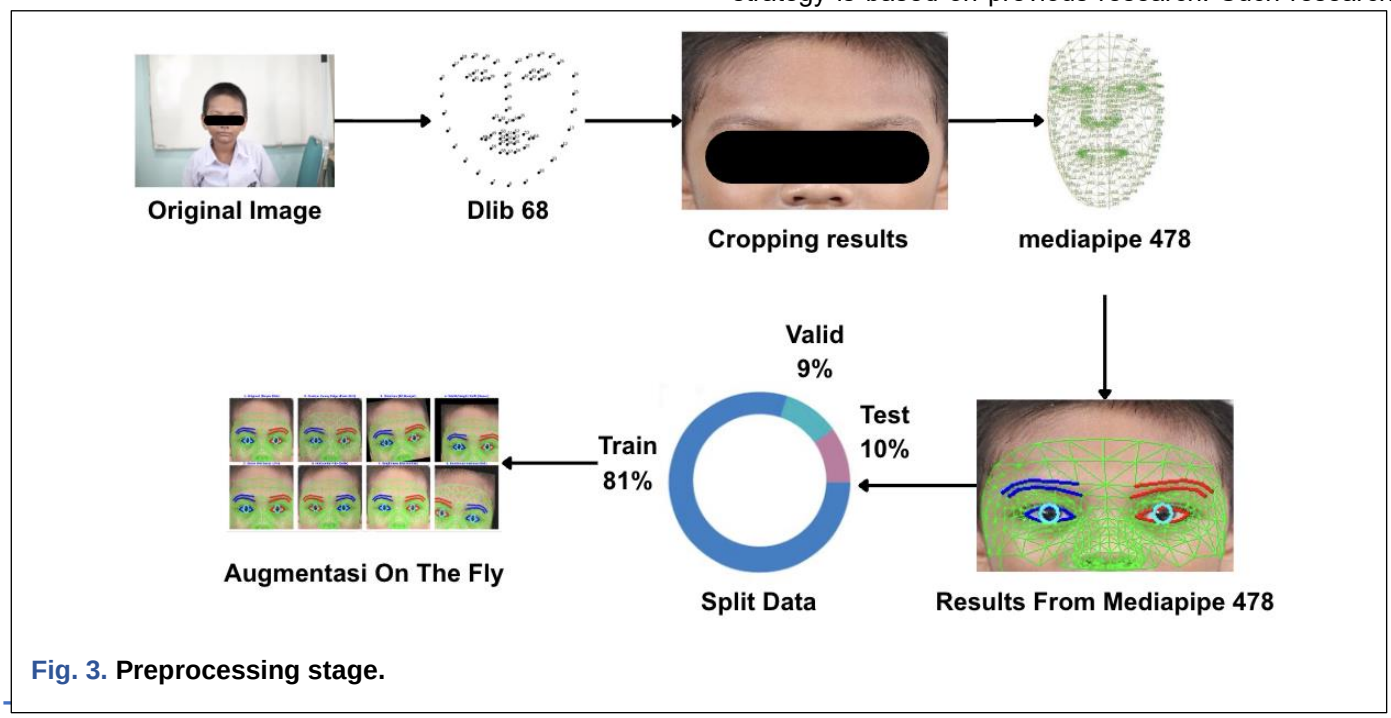

Fig. 3. Preprocessing stage.

Corresponding author: Yunidar, yunidar@usk.ac.id, Department of Electrical and Computer Engineering,Faculty of Engineering, Universitas Syiah Kuala, Darussalam, Banda Aceh, 23111, Aceh, Indonesia
DOI: https://doi.org/10.35882/jteknokes.v19i2.158

shows that combining visual landmark features produces a more discriminative spatial representation CNN architecture than using numerical coordinates alone [26].

This mapping process is carried out by transforming normalized coordinates $P(x_{Norm}, y_{Norm})$ from MediaPipe into the image pixel coordinates $P(X_{px}, Y_{px})$ via the function Eq. 1 :

$$X_{px} = x_{norm}.w, Y_{px} = y_{norm} \quad (1)$$

Where *w* and *h* are the width and height of the input image I, respectively. To emphasize the iris area, the algorithm calculates the iris center point (C_{iris}) based on the average position of *N* iris marker points via Eq. 2:

$$C(x,y) = \left(\frac{1}{N}\sum_{i=1}^{N} X_i, \frac{1}{N}\sum_{i=1}^{N} Y_i\right) \quad (2)$$

The iris radius (*R*) is determined dynamically by averaging the Euclidean distance between (C_{iris}) and all detected iris marker points via Eq. 3:

$$R = \frac{1}{N}\sum_{i=1}^{N}\sqrt{(X_i - C_x)^2 + (Y_i - C_y)^2} \quad (3)$$

In cases where iris detection fails or is unstable ($R \leq 2$), the system applies a fallback protocol by estimating the iris radius as 25% of the eye bounding box width (W_{eye}), which is defined as R_{est} = 0.25 x W_{eye}. via Eq. 4:

$$R_{est} = 0.25 \text{ x } W_{eye} \quad (4)$$

This approach ensures consistency of visual features across datasets despite variations in pose or closed-eye conditions, as well as serving as an implicit normalization method to suppress unwanted intra-class variability, such as differences in skin color or lighting [20] [36]. Fig. 3 illustrates the complete data transformation from raw images to geometric maps.

D. Split Data Strategy

In the final preprocessing stage, the dataset is partitioned into three mutually exclusive subsets. The total dataset, consisting of 1,278 images, was divided into an 81:9:10 ratio, namely: 81% for training (1,002 images), 9% for validation (112 images), and 10% for testing (124 images). Formally, if *D* represents the total dataset, then this division satisfies the condition $D = D_{train} \cup D_{val} \cup D_{test}$ with $D_{train} \cap D_{val} \cap D_{test}$ = 0 This strategy adopts a dominant allocation scheme for training data to maximize the model's ability to learn complex hierarchical features from visual landmark representations. [25] [30]. Before division, image files in each class are randomly shuffled using a permutation algorithm to ensure a uniform distribution of variability. The test dataset (124 images) is treated as a completely isolated hold-out set (*I*). This data is never involved in weight training or hyperparameter tuning. This physical isolation of the data folder is intended to mitigate the risk of data leakage, ensuring that the final performance metrics truly reflect the model's generalization to real world data that has never been seen before [36]. To validate this experimental design and objectively evaluate model performance, an average metric was calculated from the confusion matrix. The mathematical formulas for calculating overall accuracy (Acc) and sensitivity (Recall) are explicitly defined in Eq. 12 and Eq. 14, respectively, in the metrics evaluation section. The use of this protocol, combined with validation set monitoring, effectively reduces the risk of overfitting and guarantees the reliability of experimental results [19].

E. On-the-Fly Data Augmentation

Given the scarcity of data in medical image analysis [18] [37], we implemented a direct data augmentation technique using a dynamic generator. This method stochastically manipulates input images within each training batch without increasing physical storage requirements. The transformations performed include rotation (10°), translation (10%), zoom (10%), horizontal flip, and brightness adjustment to enrich photometric variability. This approach strategically increases the model's invariance to facial pose variations and lighting fluctuations, effectively preventing overfitting by encouraging the learning of persistent structural features. The effectiveness of augmentation techniques in improving the accuracy and robustness of models for ASD diagnosis, particularly in capturing differences in facial features that are difficult to distinguish by simple visual inspection, has been empirically validated in previous research [34] and in a recent comparative study of CNN architectures [25].

F. Classification Using VGG19 Architecture

This study applies VGG19, a pre-trained Convolutional Neural Network (CNN) architecture, on the ImageNet dataset for landmark visualization image classification. VGG19 was chosen for its deep architecture with 19 layers and its robust, consistent performance in medical image recognition tasks [24] [38] [30]. Fig.3 presents the modified model architecture. The network processes an input image I (224 × 224 pixels, RGB) using a sequence of convolutional blocks. The fundamental operation in this layer is 2D convolution, where a kernel *w* of size 3 x 3 is shifted over the input I with a stride of 1 pixel. This design allows for the capture of fine geometric details such as eyebrow curvature and eye shape. The convolution output at position *(i, j)* is defined as Eq.5.

$$y_{i,j}^{(k)} = \sigma\left(\sum_m \sum_n w_{m,n}^{(k)} \cdot I_i + m, j + n + b^{(k)}\right) \quad (5)$$

Where $b^{(k)}$ is the bias and σ is the ReLU activation function *(f(x) = max(0, x)).* This design allows for the capture of fine geometric details, such as eyebrow curvature and eye shape, while preserving hierarchical spatial information from low to high levels [32]. After passing through five convolutional blocks, a Max Pooling operation is performed to reduce the spatial dimensions while preserving the dominant features, as in Eq.6.

$$y_{i,j} = \max_{(m,n)\in R_{i,j}}(x_{m,n}) \quad (6)$$

After going through five convolution blocks, the 7 x 7 x 512 feature map is transformed into a 1D vector using a Global Max Pooling layer [39]. The main modification in this study lies in the classification section (Custom Head), which replaces the original fully connected layer for computational efficiency. The feature vector is processed by two Dense layers (128 and 256 neurons, respectively). To mitigate overfitting, a Dropout

Corresponding author: Yunidar, yunidar@usk.ac.id, Department of Electrical and Computer Engineering,Faculty of Engineering, Universitas Syiah Kuala, Darussalam, Banda Aceh, 23111, Aceh, Indonesia
DOI: https://doi.org/10.35882/jteknokes.v19i2.158

Fig. 4. VGG19 model training: (a) Accuracy curve, (b) Loss curve.

mechanism is applied after each Dense layer with a probability of P = 0.45, which effectively overcomes the limitations of limited medical datasets [36] [39]. This operation is modeled by Eq. 7.

$$\hat{y} = r.y, \quad r \sim Bernoulip(P) \tag{7}$$

The final output layer consists of one neuron with a Sigmoid activation function to produce a binary classification probability P as Eq. 8.

$$S(z) = \frac{1}{1+e^{-z}} \tag{8}$$

The training procedure uses transfer learning by leveraging the weights of the pre-trained VGG19 model trained on the ImageNet dataset. Formally, the model parameters θ are divided into two parts: θ_{base}, which represents the backbone layer (feature extraction), and θ_{head}, which represents the custom classification layer (Custom Head). In this study, a layer-freezing mechanism is applied to the backbone layer to preserve the learned visual features. This is expressed mathematically by keeping the weights of θ_{base} constant during the training phase (Eq. 9).

$$\Delta\theta_{base} = 0 \tag{9}$$

The weight update is only performed on the θ_{head} parameter through an optimization process. To minimize prediction error, the Binary Crossentropy (*L*) loss function is used, which measures the difference between the predicted probability *P* and the actual label *y* for each input *I*, as defined in Eq. 10.

$$L = -\frac{1}{N}\sum_{i=1}^{N}[y_i \log(P_i) + (1-y_i)\log(1-P_i)] \tag{10}$$

The optimization process to minimize L is performed using the Adam optimizer. The weight update at each iteration t is defined as Eq.11.

$$\theta_{t+1} = \theta_t - \eta \cdot \frac{\breve{m}_t}{\sqrt{\breve{v}_t}+\epsilon} \tag{11}$$

Here, η is the learning rate set to 0.0001, and $\breve{m}_t$ and $\breve{v}_t$ are estimates of the first (mean) and second (unbiased variance) moments of the gradient, using momentum hyperparameters β_1 = 0.9 and β_2 = 0.999. This approach allows the model to adapt the high level feature mapping of input *I* into class probabilities *P* while preserving the established spatial feature representation. [15] [37] [40]. To ensure stable training results over 150 epochs, the convergence criteria were closely monitored. Mathematically, the model is considered to have reached convergence when the gradient of the loss function with respect to the weight parameter θ approaches zero, as expressed in Eq. 12:

$$\frac{\partial L}{\partial \theta} \tag{12}$$

This condition indicates that the model has reached a local minimum point on the loss surface, where further weight updates no longer provide a significant reduction in loss. In this study, convergence is ensured through observing the training and validation loss curves. If the validation loss does not decrease significantly over a specified number of epochs (early stopping criteria), the model is declared to have converged. This ensures that the resulting model is stable and has optimal generalization capabilities for input data *I* [19] [25].

G. Evaluation of Metrics

Model performance is evaluated using confusion matrices and derived metrics on test data. This 2 x 2 table summarizes the predictions for the Autistic and Normal classes by categorizing the results into four fundamental components: true positives, true negatives, false positives, and false negatives.[24]:

- True Positives (TP): Images of children with ASD correctly identified as Autistic.
- True Negatives (TN): Number of normal child images correctly identified as the Normal class.
- False Positives (FP): Normal child images incorrectly classified as Autistic (false alarms).
- False Negative (FN): Images of children with ASD are incorrectly classified as Normal (missed detections).

Five evaluation metrics are derived from the confusion matrix to comprehensively assess model performance:

a) Accuracy measures how well the model classifies cases by dividing the number of correctly identified

Corresponding author: Yunidar, yunidar@usk.ac.id, Department of Electrical and Computer Engineering,Faculty of Engineering, Universitas Syiah Kuala, Darussalam, Banda Aceh, 23111, Aceh, Indonesia
DOI: https://doi.org/10.35882/jteknokes.v19i2.158

ASD and Normal instances by the total number of cases Eq. (13):

$$Accuracy = \frac{TP+TN}{TP+TN+FN+FP} \times 100 \quad (13)$$

b) Precision measures the proportion of ASD predictions that are correct, minimizing false positives and increasing diagnostic confidence Eq. (14):

$$Precision = \frac{TP}{TP+FP} \times 100 \quad (14)$$

c) Recall, or sensitivity, measures a model's ability to correctly identify all ASD cases in a dataset, which is crucial in a medical context for minimizing the risk of missing positive cases Eq. (15):

$$Recall = \frac{TP}{TP+FN} \times 100 \quad (15)$$

d) The F1 Score is the harmonic mean of Recall and Precision, balancing these metrics. It gives a more objective evaluation than accuracy, especially when precision and sensitivity are imbalanced Eq. (16):

$$F1\ Score = 2 \times \frac{Recall \times Precision}{Recall + Precision} \quad (16)$$

e) Th The Area Under the Receiver Operating Characteristic Curve (AUC-ROC) is evaluated by plotting the True Positive Rate (TPR) against the False Positive Rate (FPR) at various decision thresholds. TPR is defined as the true positive ratio (the same as Recall), while FPR is the false positive ratio calculated as FP / (FP + TN). The AUC value represents the probability P of the model in separating classes accurately, which is mathematically calculated through the integral [41] [24], as formulated in Eq. (17):

$$AUC = \int_0^1 TPR(FPR)\ d\ (TPR) \quad (17)$$

H. Statistical Analysis

To ensure the reliability of the experimental results, formal statistical tests were carried out. The validity of the model accuracy is measured using a 95% Confidence Interval (CI) with a normal approximation method based on the number of input samples (N = 124), such as Eq. 18:

$$CI = P \pm Z\sqrt{\frac{P(1-P)}{N}} \quad (18)$$

Where *P* is the accuracy value, and *Z* is the standard score (1.96). In addition, hypothesis testing is carried out to calculate the *P value* to determine whether the model performance is statistically significant compared to random classification (*p*=0.5), such as Eq. 19:

$$P(k;N,p) = \binom{N}{K} p^k (1-p)^{N-k} \quad (19)$$

Where k is the number of correct predictions, results were considered significant if the P value < 0.05, and a bootstrapping technique with 1,000 iterations was also applied to produce metric estimates that were stable against data variance [41] [45].

I. Statistical Analysis

To provide clinical transparency, this study applied the Gradient-weighted Class Activation Mapping (Grad-CAM) method. This method visualizes the spatial features at input I that most contribute to the model's classification decision through computing gradients in the last convolutional layer. The neuron importance weight σ_k^c is calculated based on the average gradient of class scores over the feature map, as formulated in Eq.20.

$$\sigma_k^c = \frac{1}{z}\sum_i \sum_j \frac{\partial y^c}{\partial A_{i,j}^k} \quad (20)$$

Where y^c is the score for class *c*, A^k is the *k* feature map, and *Z* is the number of pixels in the feature map. The weights σ_k^c are then multiplied by the feature map A^k and passed through the ReLU activation function to produce the final Grad-CAM map, $L_{Grad-cam}^c$ as in Eq. 21:

$$L_{Grad-cam}^c = ReLu(\sum_k \sigma_k^c\ A^k) \quad (21)$$

This visualization ensures that the model consistently pays attention to key biomarker areas of ASD in children [46] [47]

3. RESULTS

A. Model Training Dynamics

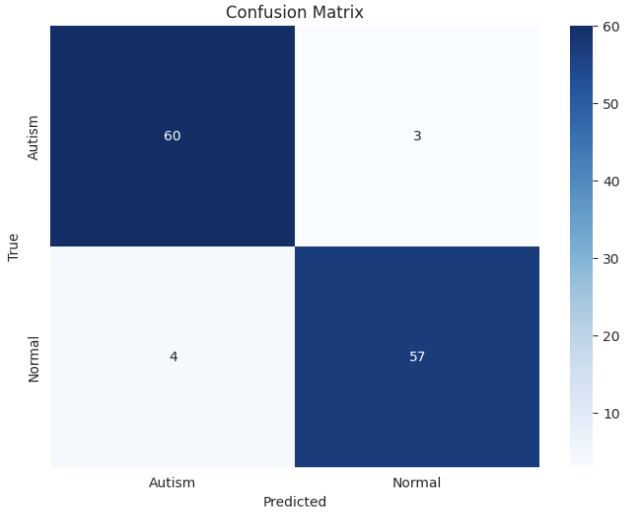

Fig. 5. Confusion Matrix on Test Data for Learning Rate 0.0001.

Model training was carried out for 150 epochs using the Adam optimizer and an initial learning rate of $1\ x\ 10^{-4}$. Learning stability and convergence were closely monitored throughout training. Accuracy and loss curves during training and validation are shown in Fig. 4. Analysis of Fig. 4(a) shows that the validation accuracy (red line) increases exponentially over the first 15 epochs, then reaches a stable plateau of 93%-95%. This phenomenon is linearly correlated with a drastic decrease in the loss curve in Fig. 4(b), which reaches a minimum below 0.20. The very narrow gap between the training and validation curves indicates that the model has robust generalization capabilities and successfully mitigates the risk of overfitting, an achievement

Corresponding author: Yunidar, yunidar@usk.ac.id, Department of Electrical and Computer Engineering,Faculty of Engineering, Universitas Syiah Kuala, Darussalam, Banda Aceh, 23111, Aceh, Indonesia
DOI: https://doi.org/10.35882/jteknokes.v19i2.158

supported by the implementation of the Dropout strategy and effective data augmentation [36] [39].

B. Classification Performance Analysis

To objectively validate the model's reliability, evaluation was performed on a test data set consisting of 124 previously unseen images. The distribution of predicted results against ground truth labels is shown in the Confusion Matrix in Fig. 5. Based on Fig. 5, the model demonstrates superior discriminatory performance. Of the total 63 samples in the 'Autistic' class, the model correctly identified 60 (True Positive), leaving only 3 errors (False Negative). Meanwhile, in the 'Normal' class, the model correctly identified 57 of 61 samples (True Negatives). This low false-negative rate is crucial in the context of medical applications, as it ensures the sensitivity of screening tools in detecting positive cases [24] [30]. A quantitative summary of the performance metrics is presented in detail in Table 1. The proposed model achieves an overall accuracy of 94.35%. To ensure the reliability of these results, formal statistical tests were carried out. Based on the test data sample size (N=124), the model produces a 95% Confidence Interval (CI) between 90.29% and 98.41% (Eq. 17). Hypothesis testing against random chance yields a P value < 0.001 (5.55×10^{-26}) (Eq. 18), confirming that the model performance is statistically significant and not the result of chance

Furthermore, the model's stability was validated using a bootstrapping technique with 1,000 resampling iterations. The bootstrapping results show a consistent average accuracy of 94.34% with a 95% CI range between 90.32% (lower limit) to 98.39% (upper limit). This consistency proves that the model has robust generalization capabilities over input sample variations I and effectively reduces the risk of overfitting [41] [45]. Recall (Sensitivity) was 95.24%. The model showed a very high ability to identify subjects with ASD. Precision was 93.75%, reflecting high confidence in positive predictions. [42] [43].

Table 1. Summary of Model Performance Evaluation Metrics

Metric Parameter	Value (%)
Accuracy	94.35
Recall	95.24
Precision	93.75
F1-Score	94.49
AUC Score	98.31

To complement the threshold-based metrics, the separability of the model was further validated using the Receiver Operating Characteristic (ROC) curve in Fig. 6. The area under the curve (AUC) reached 0.9831, a value close to 1.0, confirming that the landmark based VGG19 model has a very high probability of distinguishing between the autistic and normal classes at various decision thresholds [41] [44]. Finally, to provide deep clinical transparency, Grad-CAM visualization was implemented to identify marker feature areas that most influence classification results. Results in Fig. 6 consistently show that the VGG19 model assigns the highest gradient weights to the periorbital (eyes and eyebrows) and forehead areas. These gradient based computations prove that the model's classification decisions are based on neurobiologically relevant facial landmark biomarkers, not on background artifacts. This consistency of spatial focus in input area I strengthens clinical confidence in the reliability of the proposed model [41] [46].

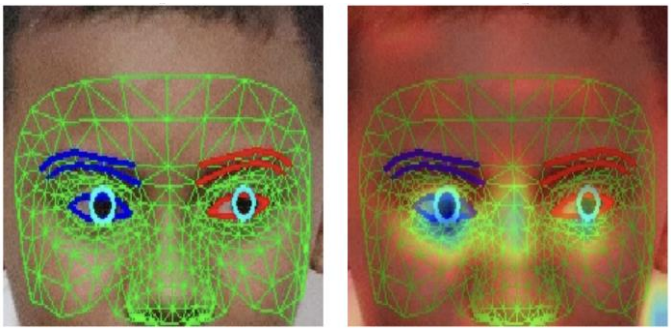

Fig. 6. Visualizing Model Interpretability Using Grad-CAM.

C. ROC and AUC Analysis

In addition to threshold based metrics, the model's separability was validated using the Receiver Operating Characteristic (ROC) curve shown in Fig. 7. The area under the curve (AUC) was 0.9831. This value, which is close to the ideal 1.0, indicates that the VGG19 model trained on eye and forehead landmarks has a very high probability of accurately distinguishing between the autistic and normal classes across a wide range of decision thresholds. This result confirms the model's stability and reliability, compared with methods with lower AUCs [41] [44].

4. DISCUSSION

A. Training Dynamics and Stability

As visualized in Fig. 4, the model training dynamics provide comprehensive insights into the learning stability of the modified VGG19 architecture. The training accuracy curve (blue line) shows a sharp logarithmic increase in the early phase, reaching a plateau above 90%, indicating that the model backbone effectively extracts discriminative features from visual landmark representations. The most important indicator is the behavior of the validation curve (red line), which moves synchronously with the training curve, maintaining a very narrow generalization gap. This simultaneous convergence, accompanied by a low loss value (L < 0.20), indicates that the model successfully learns common geometric facial patterns rather than simply memorizing the training data. This stability of the training process is mathematically confirmed by the convergence criterion defined in Eq.12, where the gradient of the loss function with respect to the weight parameter θ approaches zero, indicating that the model has reached

Corresponding author: Yunidar, yunidar@usk.ac.id, Department of Electrical and Computer Engineering,Faculty of Engineering, Universitas Syiah Kuala, Darussalam, Banda Aceh, 23111, Aceh, Indonesia
DOI: https://doi.org/10.35882/jteknokes.v19i2.158

an optimal local minimum. This confirms the success of the regularization strategy via Dropout layers (0.45) and dynamic data augmentation in reducing the risk of overfitting.

B. Limitations and Future Works

Final validation on unseen data confirms the model's reliability. As illustrated in the confusion matrix (Fig. 5), the model achieved 94.35% accuracy, with a very low misclassification rate of 7 errors out of 124 images. The statistical significance of this performance is validated by a 95% Confidence Interval (CI) of 90.29% to 98.41% (Equation 18) and a P-value < 0.001 (Equation 19), confirming that the results were not due to random chance. Clinically, the most prominent metric was Recall (Sensitivity) at 95.24%. In the development of clinical decision support systems (CDS), sensitivity is a priority parameter because failure to detect false negatives can delay early intervention, which is crucial for child development. The AUC score of 0.9831 (Fig. 7) further supports these findings, demonstrating superior and consistent class separation. In addition, the Grad-CAM implementation in Figure 6 provides in-depth clinical transparency by identifying that the highest gradient weights are assigned to the periorbital and forehead areas, as mathematically formulated in Eq. 20 and Eq. 21.

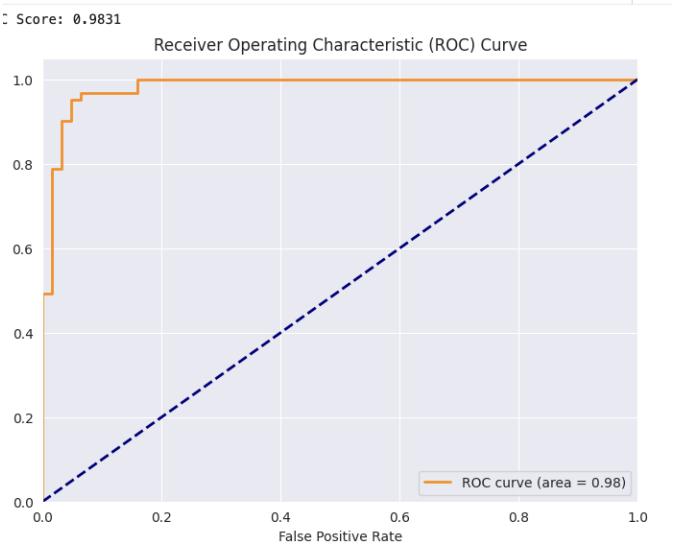

Fig. 7. ROC curve

5. CONCLUSION

This research aims to design and implement a hybrid method using a modified VGG19 architecture to detect ASD through landmark visualizations focused on the eye and forehead areas, and to evaluate the superiority of this approach over conventional full-face methods. The results indicate that this innovative early-detection system successfully integrates the VGG19 CNN model with MediaPipe facial landmark visualization to eliminate visual noise, achieving 94.35% accuracy and an AUC score of 0.9831. The most significant clinical finding is the achieved sensitivity (recall) of 95.24%, demonstrating the system's reliability in minimizing the risk of false-negative detections. The robustness of these results is further supported by formal statistical validation, which yielded a significant P-value and stable confidence intervals, and by Grad-CAM analysis, which confirmed that the model consistently focused on relevant periorbital biomarkers. This implementation validates that focusing on the eye and forehead areas is a robust biomarker approach for objective automated classification. In the future, research and development can focus on using purely numerical coordinate data to develop a more lightweight model and integrate it into a mobile application, so that the results of this study can be transformed into a practical, easily accessible, non-invasive screening tool for the wider community to support more effective early intervention.

REFERENCES

[1] O. I. Talantseva *dkk.*, "The global prevalence of autism spectrum disorder: A three-level meta-analysis," *Front. Psychiatry*, vol. 14, hlm. 1071181, Feb 2023, doi: 10.3389/fpsyt.2023.1071181.

[2] N. Salari *dkk.*, "The global prevalence of autism spectrum disorder: a comprehensive systematic review and meta-analysis," *Ital. J. Pediatr.*, vol. 48, no. 1 hlm. 112, Des 2022, doi: 10.1186/s13052-022-01310-w.

[3] R. Revilla *dkk.*, "Facial Emotion Recognition Trainings for Children and Adolescents: A Transdiagnostic Systematic Review and Meta-Analysis," *Clin. Psychol. Psychother.*, vol. 32, no. 4, hlm. e70116, Jul 2025, doi: 10.1002/cpp.70116

[4] C. Lord *dkk.*, "The Lancet Commission on the future of care and clinical research in autism," *The Lancet*, vol. 399, no. 10321, hlm. 271–334, Jan 2022, doi: 10.1016/S0140-6736(21)01541-5.

[5] K. Allen, J. Harrington, L. B. Quetsch, J. Masse, C. Cooke, dan J. F. Paulson, "Parent–Child Interaction Therapy for Children with Disruptive Behaviors and Autism: A Randomized Clinical Trial," *J. Autism Dev. Disord.*, vol. 53, no. 1, hlm. 390–404, Jan 2023, doi: 10.1007/s10803-022-05428-y.

[6] I. Scarcella *dkk.*, "Information and communication technologies-based interventions for children with autism spectrum conditions: a systematic review of randomized control trials from a positive technology perspective," *Front. Psychiatry*, vol. 14, hlm. 1212522, Jul 2023, doi: 10.3389/fpsyt.2023.1212522.

[7] S. Cored Bandrés, S. Vázquez Toledo, dan M. Liesa Orús, "Social skills, autism and technologies: An analysis of the effectiveness of this triad," *Educ. Inf. Technol.*, vol. 28, no. 8, hlm. 9285–9304, Agu 2023, doi: 10.1007/s10619-022-10990-0.

[8] N. Stuart, A. Whitehouse, R. Palermo, E. Bothe, dan N. Badcock, "Eye Gaze in Autism Spectrum

Corresponding author: Yunidar, yunidar@usk.ac.id, Department of Electrical and Computer Engineering,Faculty of Engineering, Universitas Syiah Kuala, Darussalam, Banda Aceh, 23111, Aceh, Indonesia
DOI: https://doi.org/10.35882/jteknokes.v19i2.158

Disorder: A Review of Neural Evidence for the Eye Avoidance Hypothesis," *J. Autism Dev. Disord.*, vol. 53, no. 5, hlm. 1884–1905, Mei 2023, doi: 10.1007/s10803-022-05443-z.

[9] M. Rudling, P. Nyström, G. Bussu, S. Bölte, dan T. Falck-Ytter, "Infant responses to direct gaze and associations to autism: A live eye-tracking study," *Autism*, vol. 28, no. 7, hlm. 1677–1689, Jul 2024, doi: 10.1177/13623613231203037.

[10] K. Rezaee, H. Attar, dan M. Khosravi, "A review of machine learning-based methods for automatically detecting autism spectrum disorder in children's faces," dalam *2023 2nd International Engineering Conference on Electrical, Energy, and Artificial Intelligence (EICEEAI)*, Zarqa, Jordan: IEEE, Des 2023, hlm. 1–5. doi: 10.1109/EICEEAI60672.2023.10590257.

[11] F. Rosindo Daher De Barros, C. Novais F. Da Silva, G. De Castro Michelassi, H. Brentani, F. L. S. Nunes, dan A. Machado-Lima, "Computer aided diagnosis of neurodevelopmental disorders and genetic syndromes based on facial images – A systematic literature review," *Heliyon*, vol. 9, no. 10, hlm. e20517, Okt 2023, doi: 10.1016/j.heliyon.2023.e20517.

[12] D. Mukherjee *dkk.*, "Digital tools for direct assessment of autism risk during early childhood: A systematic review," *Autism*, vol. 28, no. 1, hlm. 6–31, Jan 2024, doi: 10.1177/13623613221133176.

[13] M. Sobieski, A. Sobieska, M. Sekułowicz, dan M. M. Bujnowska-Fedak, "Tools for early screening of autism spectrum disorders in primary health care – a scoping review," *BMC Prim. Care*, vol. 23, no. 1, hlm. 46, Des 2022, doi: 10.1186/s12875-022-01645-7.

[14] S. Zhang, S. Wang, R. Liu, H. Dong, X. Zhang, dan X. Tai, "A bibliometric analysis of research trends of artificial intelligence in the treatment of autistic spectrum disorders," *Front. Psychiatry*, vol. 13, hlm. 967074, Agu 2022, doi: 10.3389/fpsyt.2022.967074.

[15] B. Sistaninejhad, H. Rasi, dan P. Nayeri, "A Review Paper about Deep Learning for Medical Image Analysis," *Comput. Math. Methods Med.*, vol. 2023, no. 1, hlm. 7091301, Jan 2023, doi: 10.1155/2023/7091301.

[16] M. Li, Y. Jiang, Y. Zhang, dan H. Zhu, "Medical image analysis using deep learning algorithms," *Front. Public Health*, vol. 11, hlm. 1273253, Nov 2023, doi: 10.3389/fpubh.2023.1273253.

[17] M. Melinda, F. H. Juwono, I. K. A. Enriko, M. Oktiana, S. Mulyani, dan K. Saddami, "Application of continuous wavelet transform and support vector machine for autism spectrum disorder electroencephalography signal classification," *Radioelectron. Comput. Syst.*, no. 3, hlm. 73–90, Sep 2023, doi: 10.32620/reks.2023.3.07.

[18] M. Melinda, F. Arnia, A. Yafi, N. A. C. Andryani, dan I. K. A. Enriko, "Design and Implementation of Mobile Application for CNN-Based EEG Identification of Autism Spectrum Disorder".

[19] A. W. Salehi *dkk.*, "A Study of CNN and Transfer Learning in Medical Imaging: Advantages, Challenges, Future Scope," *Sustainability*, vol. 15, no. 7, hlm. 5930, Mar 2023, doi: 10.3390/su15075930.

[20] A. A. Mukhlif, B. Al-Khateeb, dan M. A. Mohammed, "An extensive review of state-of-the-art transfer learning techniques used in medical imaging: Open issues and challenges," *J. Intell. Syst.*, vol. 31, no. 1, hlm. 1085–1111, Sep 2022, doi: 10.1515/jisys-2022-0198.

[21] H. E. Kim, A. Cosa-Linan, N. Santhanam, M. Jannesari, M. E. Maros dan T. Ganslandt, "Transfer learning for medical image classification: a literature review," *BMC Med. Imaging*, vol. 22, no. 1, hlm. 69, Des 2022, doi: 10.1186/s12880-022-00793-7.

[22] G. Quatrosi *dkk.*, "Cranio-Facial Characteristics in Autism Spectrum Disorder: A Scoping Review," *J. Clin. Med.*, vol. 13, no. 3, hlm. 729, Jan 2024, doi: 10.3390/jcm13030729.

[23] M. Melinda, M. Oktiana, Y. Nurdin, I. Pujiati, M. Irhamsyah, dan N. Basir, "Performance of Shuffle Net and VGG-19 Architectural Classification Models for Face Recognition in Autistic Children," *Int. J. Adv. Sci. Eng. Inf. Technol.*, vol. 13, no. 2, hlm. 674–680, Apr 2023, doi: 10.18517/ijaseit.13.2.18274.

[24] Md. F. Rabbi *dkk.*, "Autism Spectrum Disorder Detection Using Transfer Learning with VGG 19, Inception V3 and DenseNet 201," dalam *Recent Trends in Image Processing and Pattern Recognition*, vol. 1704, K. Santosh, A. Goyal, D. Aouada, A. Makkar, Y.-Y. Chiang, dan S. K. Singh, Ed., dalam Communications in Computer and Information Science, vol. 1704. , Cham: Springer Nature Switzerland, 2023, hlm. 190–204. doi: 10.1007/978-3-031-23599-3_14.

[25] J. Junidar, M. Melinda, D. D. Diannuari, D. D. Acula, dan Z. Zainal, "Face autistic classification based on thermal using image ensemble learning of VGG-19, ResNet50v2, and EfficientNet," *Radioelectron. Comput. Syst.*, vol. 2025, no. 1, hlm. 153–164, Feb 2025, doi: 10.32620/reks.2025.1.11.

[26] M. A. Witherow, M. D. Samad, N. Diawara, dan K. M. Iftekharuddin, "Facial landmark feature fusion in transfer learning of child facial expressions," dalam *Applications of Machine Learning 2022*, M. E. Zelinski, T. M. Taha, dan J. Howe, Ed., San Diego, United States: SPIE, Okt 2022, hlm. 34. doi: 10.1117/12.2641898.

[27] S. Poudel *dkk.*, "Autism Spectrum Disorder Detection using Facial Landmark Detection and Artificial Neural Network".

[28] A. Lakkapragada *dkk.*, "The Classification of Abnormal Hand Movement to Aid in Autism Detection: Machine Learning Study," *JMIR*

Corresponding author: Yunidar, yunidar@usk.ac.id, Department of Electrical and Computer Engineering,Faculty of Engineering, Universitas Syiah Kuala, Darussalam, Banda Aceh, 23111, Aceh, Indonesia
DOI: https://doi.org/10.35882/jteknokes.v19i2.158

Biomed. Eng., vol. 7, no. 1, hlm. e33771, Jun 2022, doi: 10.2196/33771.
[29] R. Mohan, S. Kadry, V. Rajinikanth, A. Majumdar, dan O. Thinnukool, "Automatic Detection of Tuberculosis Using VGG19 with Seagull-Algorithm," *Life*, vol. 12, no. 11, hlm. 1848, Nov 2022, doi: 10.3390/life12111848.
[30] L. K. Gaddala *dkk.*, "Autism Spectrum Disorder Detection Using Facial Images and Deep Convolutional Neural Networks," *Rev. Intell. Artif.*, vol. 37, no. 03, hlm. 801–806, Jun 2023, doi: 10.18280/ria.370329.
[31] M. Z. Al-Taie, E. Sabeeh, dan S. Sabeeh, "Comparative Deep Learning–Based Facial Image Analysis for Early Autism Prediction in School-Aged Children," vol. 4, no. 1, 2025.
[32] M. J. Awan *dkk.*, "Image-Based Malware Classification Using VGG19 Network and Spatial Convolutional Attention," *Electronics*, vol. 10, no. 19, hlm. 2444, Okt 2021, doi: 10.3390/electronics 10192444.
[33] H. Alkahtani, T. H. H. Aldhyani, dan M. Y. Alzahrani, "Deep Learning Algorithms to Identify Autism Spectrum Disorder in Children-Based Facial Landmarks," *Appl. Sci.*, vol. 13, no. 8, hlm. 4855, Apr 2023, doi: 10.3390/app13084855.
[34] M.S.Alam dkk., "Efficient Deep Learning-
Based Data-Centric Approach for Autism Spectrum
Disorder Diagnosis from Facial Images Using Ex plainable AI," *Technologies*, vol. 11, no. 5, hlm.11 5, Agu 2023, doi: 10.3390/technologies11050115.
[35] M. E. Tezcan, A. E. Ataş, dan H. Ferahkaya, "Can optic nerve morphology in children with autism spectrum disorder be associated with atypical visual-sensory behaviors?," *Front. Psychiatry*, vol. 16, hlm. 1619695, Agu 2025, doi: 10.3389/fpsyt.2025.1619695.
[36] M. S. Alam, M. M. Rashid, R. Roy, A. R. Faizabadi, K. D. Gupta, dan M. M. Ahsan, "Empirical Study of Autism Spectrum Disorder Diagnosis Using Facial Images by Improved Transfer Learning Approach," *Bioengineering*, vol. 9, no. 11, hlm. 710, Nov 2022, doi: 10.3390/bioengineering9110710.
[37] M. Tsuneki, "Deep learning models in medical image analysis," *J. Oral Biosci.*, vol. 64, no. 3, hlm. 312–320, Sep 2022, doi: 10.1016/j.job.2022.03.003.
[38] A. Faghihi, M. Fathollahi, dan R. Rajabi, "Diagnosis of Skin Cancer Using VGG16 and VGG19 Based Transfer Learning Models," 1 April 2024, *arXiv*: arXiv:2404.01160. doi: 10.48550/arXiv.2404.01160.
[39] "Modified VGG-19 Deep Learning Strategies for Parkinson's Disease Diagnosis - A Comprehensive Review and Novel Approach," *J. Angiother.*, vol. 8, no. 3, Mar 2024, doi: 10.25163/angiotherapy.839559.
[40] Z. Zhao, L. Alzubaidi, J. Zhang, Y. Duan, dan Y. Gu, "A comparison review of transfer learning and self-supervised learning: Definitions, applications, advantages and limitations," *Expert Syst. Appl.*, vol. 242, hlm. 122807, Mei 2024, doi: 10.1016/j.eswa.2023.122807.
[41] K. K. Mujeeb Rahman dan M. M. Subashini, "Identification of Autism in Children Using Static Facial Features and Deep Neural Networks," *Brain Sci.*, vol. 12, no. 1, hlm. 94, Jan 2022, doi: 10.3390/brainsci12010094.
[42] A. Alias dan M. A. As'ari, "Vision Based Screening of Children with Autism Spectrum Disorders Via Deep Learning Approach," *J. Hum. Centered Technol.*, vol. 4, no. 2, hlm. 148–154, Agu 2025, doi: 10.11113/humentech.v4n2.114.
[43] Master of Engineering Management, Lamar University, Beaumont, Texas, United States of America *dkk.*, "COMPARATIVE ANALYSIS OF NEURAL NETWORK ARCHITECTURES FOR MEDICAL IMAGE CLASSIFICATION: EVALUATING PERFORMANCE ACROSS DIVERSE MODELS," *Am. J. Adv. Technol. Eng. Solut.*, vol. 04, no. 01, hlm. 01–42, Mar 2024, doi: 10.63125/feed1x52.
[44] Y. Li, W.-C. Huang, dan P.-H. Song, "A face image classification method of autistic children based on the two-phase transfer learning," *Front. Psychol.*, vol. 14, hlm. 1226470, Agu 2023, doi: 10.3389/fpsyg.2023.1226470.
[45] A. M. Al-Saadi dan D. Al-Thani, "Mobile Application to identify and recognize emotions for children with autism: A systematic review," *Front. Child Adolesc. Psychiatry*, vol. 2, hlm. 1118665, Mar 2023, doi: 10.3389/frcha.2023.1118665.
[46] A. M. Al-Saadi dan D. Al-Thani, "Mobile Applicatio H. A. Mengash *dkk.*, "Automated Autism Spectral Disorder Classification Using Optimal Machine Model".http://dx.doi.org/10.32604/cmc.2023.032729
[47] M. Radhakrishnan, K. Ramamurthy, K. K. Choudhury, D. Won, dan T. Aarthy, "Performance Analysis of Deep Learning Models for Detection of Autism Spectrum Disorder from EEG Signals". https://doi.org/10.18280/ts.380332

AUTHOR BIOGRAPHY

Arya Suyanda born on March 27th, 2003 in Banda Aceh. He is a student of Electrical and Computer Engineering Department, Universitas Syiah Kuala. His undergraduate studies focused on multimedia technology, and his research explored $H_2O$and $H_2O$with NaOH. He actively participates in class and continues to develop his knowledge in his field. Enrolled in the class of 2022, he is committed to expanding his expertise and gaining practical experience. His academic journey reflects his dedication to theoretical and applied learning, which prepares him to contribute to the

Corresponding author: Yunidar, yunidar@usk.ac.id, Department of Electrical and Computer Engineering,Faculty of Engineering, Universitas Syiah Kuala, Darussalam, Banda Aceh, 23111, Aceh, Indonesia
DOI: https://doi.org/10.35882/jteknokes.v19i2.158

e-ISSN: 2407-8964
p-ISSN: 1907-7904

advancement of technology in his field. He can be reached at arya.su@mhs.usk.ac.id.

Yunidar was born in Banda Aceh, Aceh, on June 29, 1974. She has been a lecturer at the Faculty of Engineering, Department of Electrical and Computer Engineering, Syiah Kuala University, since March 2000. After completing her undergraduate education in Physics at Syiah Kuala University, Aceh-Indonesia, in 1997, she then obtained a Master of Engineering (MT) degree in Optoelectrotechnics and Laser Applications from University of Indonesia, Jakarta-Indonesia, in 2000. She recently completed her doctoral degree program in electrical and computer engineering at Syiah Kuala University and graduated in 2025. She is also a member of IEEE. Her research interests include the implementation of biomedical engineering and sensors used in biomedical applications, including multimedia. She can be contacted at email: yunidar@usk.ac.id

Melinda was born in Bireuen, Aceh, on June 10, 1979. She received a B.Eng degree from the Department of Electrical and Computer Engineering, Faculty of Engineering, Universitas Syiah Kuala, Banda Aceh in 2002. She completed her master's degree at the Faculty of Electrical Department, University of Southampton, United Kingdom, with a concentration in field study of Radio Frequency Communication Systems in 2009. She has already completed her Doctoral degree at the Department of Electrical Engineering, Engineering Faculty of Universitas Indonesia in February 2018. She has been with the Department of Electrical Engineering, Faculty of Engineering, Universitas Syiah Kuala since 2002. She is also a member of IEEE. Her research interests include multimedia signal processing and fluctuation processing. She can be contacted at email: melinda@usk.ac.id.

Dr. Lailatul Qadri Zakaria earned her Ph.D. from the University of Southampton, U.K. She is currently a Senior Lecturer at the Centre of Artificial Intelligence (CAIT), Faculty of Information Science and Technology (FTSM), Universiti Kebangsaan Malaysia (UKM). She is also a member of the Asian Language Processing (ASLAN) research group. Her research interests include natural language processing (NLP), computational linguistics, and semantic web technologies. She has contributed to various studies on text analysis and machine learning for NLP. With extensive academic experience, she actively participates in scientific publications, research collaborations, and mentoring students in the field of artificial intelligence and language technology. She can be contacted at lailatul.qadri@ukm.edu.my

Siti Rusdiana, was born in Banda Aceh, Indonesia, on 10 September 1965. She received the B.S. degree in mathematics science from the Institut Teknologi Sepuluh Nopember, Surabaya, Indonesia, in 1988, the M.Eng. degree in mathematics science from Osaka University, Osaka, Japan, in 1998, and the Ph.D. degree in applied mathematics from Universitas Sumatera Utara, Medan, Indonesia, in 2013. She was the Chairperson of the Department of Mathematics, Universitas Syiah Kuala, Banda Aceh, Indonesia (1998 – 2004). From 2013 to 2020, she was the Head of the Laboratory for Dynamic and Optimization Applications, Department of Mathematics, Universitas Syiah Kuala, where she has been an Associate Professor with the Department of Mathematics, since 2014. She is also a member of IEEE. Her research interests in applied mathematics include optimization, operation research, data science. She can be contacted at email: siti.rusdiana@usk.ac.id

Corresponding author: Yunidar, yunidar@usk.ac.id, Department of Electrical and Computer Engineering,Faculty of Engineering, Universitas Syiah Kuala, Darussalam, Banda Aceh, 23111, Aceh, Indonesia
DOI: https://doi.org/10.35882/jteknokes.v19i2.158

e-ISSN: 2407-8964
p-ISSN: 1907-7904

Corresponding author: Yunidar, yunidar@usk.ac.id, Department of Electrical and Computer Engineering,Faculty of Engineering, Universitas Syiah Kuala, Darussalam, Banda Aceh, 23111, Aceh, Indonesia
DOI: https://doi.org/10.35882/jteknokes.v19i2.158